




Modulational instability in randomly dispersion-managed optical fiber links

Andrea Armaroli ^{1,*}, Guillaume Dujardin ², Alexandre Kudlinski,¹ Arnaud Mussot,¹
Stephan De Bièvre ³ and Matteo Conforti¹

¹Univ. Lille, CNRS, UMR 8523-PhLAM-Physique des Lasers Atomes et Molécules, F-59000 Lille, France

²Univ. Lille, Inria, CNRS, UMR 8524 - Laboratoire Paul Painlevé, F-59000 Lille, France

³Univ. Lille, CNRS, Inria, UMR 8524 - Laboratoire Paul Painlevé, F-59000 Lille, France



(Received 5 April 2023; accepted 31 July 2023; published 15 August 2023)

We study modulational instability in a dispersion-managed optical fiber system where the sign of the group-velocity dispersion is changed at uniformly distributed random distances around a reference length. We find an instability gain of stochastic origin comparable to the conventional values found in a homogeneous anomalous dispersion fiber. We develop an accurate analytical technique based on transfer matrices to estimate the instability gain from the linearized nonlinear Schrödinger equation, which is also solved numerically. The comparison of numerical and analytical results confirms the validity of our approach. Modulational instability sidebands of purely stochastic origin appear and the competition between sidebands of periodic and stochastic origin is also discussed. These results may be of interest in tailoring and controlling modulational instability sidebands for telecommunications and parametric sources. Our method can also be applied to general linear stochastic differential equations with multiplicative noise, which broadly occur in Physics.

DOI: [10.1103/PhysRevA.108.023510](https://doi.org/10.1103/PhysRevA.108.023510)

I. INTRODUCTION

Modulational instability (MI) is a pervasive phenomenon in the physics of nonlinear dispersive waves. It manifests itself as the destabilization of a uniform wave packet by the exponential growth of small harmonic perturbations around the carrier frequency of the wave packet [1]. Its study originated in hydrodynamics [2,3], but analogous phenomena were also discovered in electromagnetic waves [4] and optical fibers [5]. The main ingredients to observe MI are focusing cubic nonlinearity (such as the Kerr effect in silica optical fibers) and anomalous (negative) group-velocity dispersion (GVD).

Notwithstanding, MI can also be found in normal (positive) GVD, if higher-order dispersion [6] or birefringence [7] are considered. Moreover, in single-mode fibers, the periodic variation of GVD along the fiber length can also give rise to MI in the normal GVD regime. This effect is similar to the destabilization of a parametrically excited harmonic oscillator and is denoted as parametric MI [8–12]. Several MI sidebands appear that correspond to different resonance orders. Their frequency distance from the carrier goes as the square root of their order. Optical fibers featuring random GVD variations were also extensively studied. In the late 1990s, the exactly solvable white noise process was considered [9,13–15]. More recently, some of the present authors focused on different processes such as localized GVD kicks [16] and colored processes of low-pass and band-pass type [17].

So far, both periodic and random fluctuations have been mostly assumed to occur around an average GVD different from zero (and, more often, normal, to avoid competition with

conventional MI, which exhibits much larger MI gain). The fluctuations can be large, though.

On the contrary, systems with zero average GVD have attracted a lot of attention for the suppression of the dispersion-induced pulse broadening and the optimization of nonlinear pulse transmission [18,19]. This approach is commonly denoted as dispersion management (DM): segments of positive and negative GVD alternate along the fiber. The study of MI in periodic DM fiber links [20] shows a behavior that is different from the parametric MI: a threshold is found for the segment lengths below which no MI appears. The amplitude of GVD variations influences the MI spectral range, but has no effect on this threshold.

Here we consider random fluctuations of the DM segment lengths. While pulse propagation in a similar system was analyzed in Ref. [21], we focus here on MI by applying the technique developed in Refs. [14,16]. After deriving some analytical relations for uniformly distributed fluctuations around the periodic arrangement, we compare them to numerical solutions. We find MI bands of purely stochastic origin and characterize the transition from periodic to stochastic DM.

After stating the model equations and deriving the analytical approximations in Sec. II, we compare them to numerical results in Sec. III. The reader will find conclusions in Sec. IV.

II. ANALYTICAL APPROACH

We consider the propagation of optical pulses ruled by the nonlinear Schrödinger equation (NLSE) [18],

$$i\partial_z U - \frac{1}{2}\beta_2(z)\partial_t^2 U + \gamma|U|^2 U = 0, \quad (1)$$

where $U(t, z)$ is the complex envelope of the optical field, (t, z) are the physical time and propagation distance in a frame moving at the group velocity of the fiber mode, γ is the

*Currently at Department of Engineering, University of Ferrara, I-44122 Ferrara, Italy; andrea.armaroli@unife.it

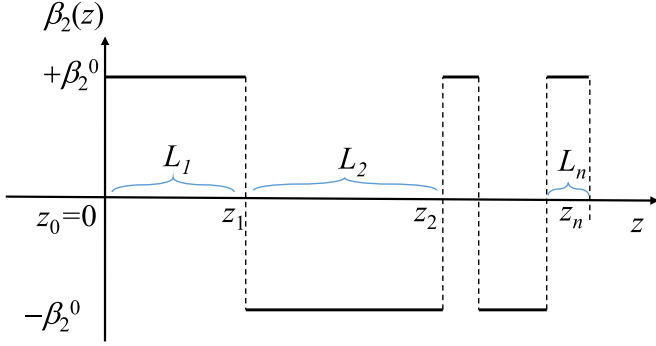


FIG. 1. Schematic representation of the GVD profile in a typical fiber realization.

(constant) nonlinear coefficient, and $\beta_2(z) = \pm\beta_2^0$ ($\beta_2^0 > 0$) is the GVD, which takes only two values. As schematically illustrated in Fig. 1, the sign changes occur at z_1, z_2, \dots, z_N , where $z_n = z_{n-1} + L_n$, $n = 1, 2, \dots, N$ and $z_0 = 0$. The lengths L_n are independent, identically distributed random variables with uniform probability distribution function in $[\bar{L}(1 - \varepsilon), \bar{L}(1 + \varepsilon)]$, where \bar{L} is the average length of one fiber segment (half of the DM period) and ε is the amplitude of the fluctuation.

Equation (1) has a continuous-wave (t -independent) solution $U_0(z) = \sqrt{P} \exp(i\gamma Pz)$. In order to study its stability, we insert in Eq. (1) the ansatz $U(z, t) = [\sqrt{P} + \check{x}_1(z, t) + i\check{x}_2(z, t)] \exp(i\gamma Pz)$, where $\check{x}_{1,2}$ are assumed to be small, then linearize and Fourier transform the resulting equation with respect to t (ω is used as the associated angular frequency detuning from the carrier U_0). We obtain

$$\frac{dx}{dz} = \begin{bmatrix} 0 & -g(z) \\ h(z) & 0 \end{bmatrix} x, \quad (2)$$

where $x \equiv (x_1, x_2)^T$ — $x_{1,2}$ are the Fourier transforms of $\check{x}_{1,2}$, functions of ω and z , $g(z) = \beta_2(z) \frac{\omega^2}{2}$, and $h(z) = g(z) + 2\gamma P$. Equation (2) is a system of stochastic differential equations (SDEs) for each value of ω .

The solution of Eq. (2) is obtained by multiplying random transfer matrices, which depend on the random variables L_n , and reads

$$x(z_N) = T_-(L_N)T_+(L_{N-1}) \dots T_-(L_2)T_+(L_1)x(z_0), \quad (3)$$

$$T_{\pm}(L_n) = \begin{bmatrix} \cos(k_{\pm}L_n) & -\mu_{\pm} \sin(k_{\pm}L_n) \\ \mu_{\pm}^{-1} \sin(k_{\pm}L_n) & \cos(k_{\pm}L_n) \end{bmatrix}, \quad (4)$$

with $k_{\pm}^2 = \pm \frac{\beta_2^0 \omega^2}{2} (\pm \frac{\beta_2^0 \omega^2}{2} + 2\gamma P)$, $\mu_{\pm} = \pm \frac{\beta_2^0 \omega^2}{2k_{\pm}}$. The sign \pm is chosen according to the sign of GVD in the corresponding segment. The wave number k_+ is always real and positive, whereas k_- is purely imaginary in the conventional MI band $0 \leq \omega \leq \sqrt{\frac{4\gamma P}{\beta_2^0}}$. Since we consider a piecewise-constant process, the Itô-Stratonovich dilemma [22] does not represent an issue for the integrals giving the transfer matrix formulation.

If the DM link is periodic, i.e., $\varepsilon = 0$, we can apply Floquet theory [20]. The unit cell of DM to be periodically replicated is represented by one positive and one negative GVD trait of length \bar{L} . The MI gain is defined as $G_1(\omega) \equiv \frac{1}{2\bar{L}} \ln \max\{|\tilde{\lambda}|, 1\}$, where $\tilde{\lambda}$ is the eigenvalue of the monodromy

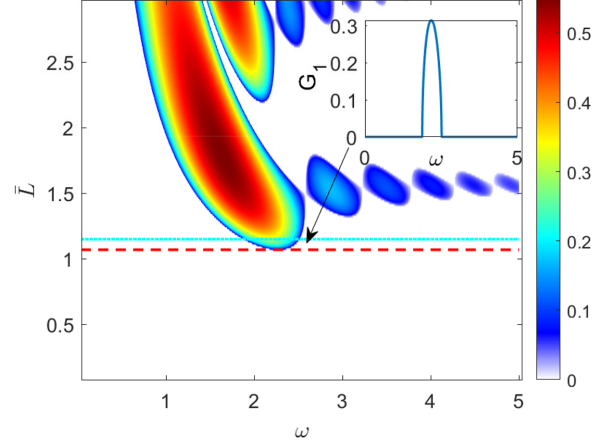


FIG. 2. False-color plot of MI gain for a periodic DM fiber as a function of dimensionless detuning ω and half period \bar{L} . The color bar shows the values of $G_1(\omega)$ (defined in the text). The red dashed horizontal line identifies $\bar{L} = 1.07$ (MI threshold), while the cyan dotted line denotes the reference value $\bar{L} = 1.15$, used in the inset and below in the random length fluctuation examples.

matrix associated to Eq. (2) of the largest modulus. This corresponds to $T_{2\bar{L}} \equiv T_-(\bar{L})T_+(\bar{L})$. For definiteness, we take $\gamma = P = \beta_2^0 = 1$, which amounts to introducing the normalized distance $z/z_{\text{nl}} \rightarrow z$, time $t/t_0 \rightarrow t$, and field $U/\sqrt{P} \rightarrow U$, where $z_{\text{nl}} = (\gamma P)^{-1}$ is the so-called nonlinear length and $t_0 = \sqrt{\beta_2^0 z_{\text{nl}}}$ is a characteristic time. The conventional MI in anomalous GVD thus reaches the maximum value of $G_{1,\text{max}} = 1$ at $\omega = \sqrt{2}$; the MI sidelobes are found in $|\omega| \leq 2$. In [20], it was observed that a critical value $\bar{L} \approx 1.07$ exists, below which $G_1 = 0$ identically. The MI gain is represented as a false-color map in Fig. 2 for $\omega \geq 0$ (for $\omega \leq 0$, we obtain its mirror image) and exhibits several lobes, in general.

For random L_n , in Refs. [14,16], it was shown that we have to resort to the Lyapunov exponent of the random linear map: the sample gain $G_S(\omega) \equiv \lim_{z_N \rightarrow \infty} \frac{1}{z_N} \ln \|T_-(L_N)T_+(L_{N-1}) \dots T_-(L_2)T_+(L_1)x(0, \omega)\|^2$ converges for almost all realizations of the fiber and is a deterministic quantity.

By taking the average of Eq. (3) and letting $N \rightarrow \infty$, we can estimate the MI gain as $G_1(\omega) \equiv \frac{1}{2\bar{L}} \ln \max\{|\lambda|, 1\}$, where λ is the largest modulus eigenvalue of $\bar{T} \equiv \langle T_- \rangle \langle T_+ \rangle$ —the angle brackets denote the expectation operation over the random lengths L_n . We can split the averages because L_n are all mutually independent. It is useful to derive by elementary integration,

$$\langle \cos(mk_{\pm}L_n) \rangle = \cos(mk_{\pm}\bar{L}) \frac{\sin(mk_{\pm}\varepsilon)}{mk_{\pm}\varepsilon}, \quad (5)$$

$$\langle \sin(mk_{\pm}L_n) \rangle = \sin(mk_{\pm}\bar{L}) \frac{\sin(mk_{\pm}\varepsilon)}{mk_{\pm}\varepsilon},$$

with $m = 1, 2, \dots$. Thus, taking $m = 1$,

$$\langle T_{\pm} \rangle = \frac{\sin k_{\pm}\varepsilon}{k_{\pm}\varepsilon} \begin{bmatrix} \cos(k_{\pm}\bar{L}) & -\mu_{\pm} \sin(k_{\pm}\bar{L}) \\ \mu_{\pm}^{-1} \sin(k_{\pm}\bar{L}) & \cos(k_{\pm}\bar{L}) \end{bmatrix}, \quad (6)$$

and \bar{T} can be easily obtained as

$$\bar{T} = \frac{\sin(k_- \varepsilon)}{k_- \varepsilon} \frac{\sin(k_+ \varepsilon)}{k_+ \varepsilon} T_{2\bar{L}}. \quad (7)$$

As common in random dynamical systems [22], we may have $G_1 = 0$ for all ω , implying that $x_{1,2}$ decay on average. Particularly, it is apparent that for $\bar{L} < 1.07$, where both eigenvalues of $T_{2\bar{L}}$ are on the unit circle, Eq. (7) implies that $G_1(\omega) = 0$ identically because \bar{T} differs from $T_{2\bar{L}}$ only by a factor no larger than one.

Nevertheless, a different kind of instability may occur, to understand which the study of second moments is required. We let $X_1 = x_1^2$, $X_2 = x_2^2$, and $X_3 = x_1 x_2$ and derive, from Eq. (2),

$$\frac{d}{dz} X = \begin{bmatrix} 0 & 0 & -2g(z) \\ 0 & 0 & 2h(z) \\ h(z) & -g(z) & 0 \end{bmatrix} X, \quad (8)$$

with $X \equiv (X_1, X_2, X_3)^T$. Equation (8) can again be solved by multiplying transfer matrices $X(z_n) = M_{\pm}(L_n)X(z_{n-1})$, with

$$M_{\pm}(L_n) = \begin{bmatrix} \cos^2(k_{\pm} L_n) & \mu_{\pm}^2 \sin^2(k_{\pm} L_n) & -\mu_{\pm} \sin(2k_{\pm} L_n) \\ \mu_{\pm}^{-2} \sin^2(k_{\pm} L_n) & \cos^2(k_{\pm} L_n) & \mu_{\pm}^{-1} \sin(2k_{\pm} L_n) \\ \frac{\mu_{\pm}^{-1}}{2} \sin(2k_{\pm} L_n) & -\frac{\mu_{\pm}}{2} \sin(2k_{\pm} L_n) & \cos(2k_{\pm} L_n) \end{bmatrix}. \quad (9)$$

The generic DM unit cell is associated to $M_-(L_n)M_+(L_{n-1})$. After Refs. [14,16], we define $G_2(\omega) \equiv \frac{1}{4\bar{L}} \ln \max\{|\kappa|, 1\}$, where κ is the largest modulus eigenvalue of $\bar{M} \equiv \langle M_- \rangle \langle M_+ \rangle$. The two factors are obtained by averaging Eq. (9) and using Eq. (5) with $m = 2$, and read

$$\langle M_{\pm} \rangle = \begin{bmatrix} \frac{1}{2} + \frac{\sin(2k_{\pm} \varepsilon) \cos(2k_{\pm} \bar{L})}{4\varepsilon k_{\pm}} & \frac{\mu_{\pm}^2}{2} - \frac{\mu_{\pm}^2 \sin(2k_{\pm} \varepsilon) \cos(2k_{\pm} \bar{L})}{4\varepsilon k_{\pm}} & -\frac{\mu_{\pm} \sin(2\varepsilon k_{\pm}) \sin(2k_{\pm} \bar{L})}{2\varepsilon k_{\pm}} \\ \frac{1}{2\mu_{\pm}^2} - \frac{\sin(2k_{\pm} \varepsilon) \cos(2k_{\pm} \bar{L})}{4\varepsilon k_{\pm} \mu_{\pm}^2} & \frac{1}{2} + \frac{\sin(2k_{\pm} \varepsilon) \cos(2k_{\pm} \bar{L})}{4\varepsilon k_{\pm}} & \frac{\sin(2\varepsilon k_{\pm}) \sin(2k_{\pm} \bar{L})}{2\varepsilon k_{\pm} \mu_{\pm}} \\ \frac{\sin(2\varepsilon k_{\pm}) \sin(2k_{\pm} \bar{L})}{4\varepsilon k_{\pm} \mu_{\pm}} & -\frac{\mu_{\pm} \sin(2\varepsilon k_{\pm}) \sin(2k_{\pm} \bar{L})}{4\varepsilon k_{\pm}} & \frac{\sin(2\varepsilon k_{\pm}) \cos(2k_{\pm} \bar{L})}{2\varepsilon k_{\pm}} \end{bmatrix}. \quad (10)$$

In the periodic limit, the monodromy matrix associated to Eq. (8) is $M_{2\bar{L}} \equiv M_-(\bar{L})M_+(\bar{L})$ and $G_2 = G_1$, for every ω . In the random case, we can easily find the expression of \bar{M} analytically by multiplying the two matrices in Eq. (10), but the expression is rather lengthy and is not reported here. In contrast to \bar{T} , it is apparent that \bar{M} is not, in general, trivially proportional to $M_{2\bar{L}}$ because of the upper-left 2×2 blocks in Eq. (10). It is also easy to verify that $\det \langle M_{\pm} \rangle = [\frac{\sin(2k_{\pm} \varepsilon)}{2k_{\pm} \varepsilon}]^2$. The use of MATHEMATICA[®] [23] allows us to obtain that the eigenvalues of $\langle M_{\pm} \rangle$ are $(1, \lambda_{\pm}, \lambda_{\pm}^*)$, with

$$\lambda_{\pm} = \frac{\sin(2k_{\pm} \varepsilon) \cos(2k_{\pm} L) + i |\sin(2k_{\pm} \varepsilon) \sin(2k_{\pm} L)|}{2k_{\pm} \varepsilon}. \quad (11)$$

This, though, does not imply anything on the eigenvalues of \bar{M} . This simple algebraic consideration implies that we may have $G_2 > 0$, even when $G_1 = 0$. Therefore, new MI sidebands of purely stochastic origin exist. The eigenvalues κ of \bar{M} may be found analytically too. Their expression is very involved, though; we thus rely on a numerical routine.

III. RESULTS

In order to assess the accuracy of our estimates, we also solve Eq. (2) numerically by taking a fixed number, $N = 20$, of fiber segments. We take $[x_1(0), x_2(0)]^T = (1, 0)$ [equivalently, $X(0)^T = (1, 0, 0)$] and multiply by the transfer matrix given by Eq. (4) N times, alternating the GVD sign according to Eq. (3). We compute $P_{\text{out}} = x_1^2(z_N) + x_2^2(z_N)$ [obviously, $P_{\text{in}} = x_1^2(0) + x_2^2(0) = 1$]. We repeat this calculation taking N_{iter} different fiber realizations, i.e., the sample size. The mean

gain is defined as either [16,17,24]

$$\bar{G}_1(\omega; N) \equiv \frac{1}{N\bar{L}} \ln \{ |\langle x_1(z_N) \rangle| + |\langle x_2(z_N) \rangle| \} \quad (12)$$

or

$$\bar{G}_2(\omega; N) \equiv \frac{1}{2N\bar{L}} \ln \left\langle \frac{P_{\text{out}}}{P_{\text{in}}} \right\rangle, \quad (13)$$

where the averages are performed on the sample and which are compared to either G_1 or G_2 , respectively.

We show, in Fig. 3, four illustrative examples of MI sidebands. We notice that in general, \bar{G}_2 converges to G_2 for $N_{\text{iter}} = 1 \times 10^6$, whereas a much larger $N_{\text{iter}} = 1 \times 10^7 - 1 \times 10^8$ is required to achieve a stable and reliable estimate of \bar{G}_1 . This can be explained by the fact that $x_{1,2}$ can be positive or negative, while $P_{\text{out}} \geq 0$. The realizations of $x_{1,2}(z_N)$ can be imagined as a set of vectors in a plane. A single realization can be a vector of extremely large norm pointing to any direction. A good estimate of \bar{G}_1 thus requires a larger sample size because the plane must be exhaustively explored to not overestimate extreme values. Increasing N makes this problem worse because the accumulated growth is larger in longer domains.

We notice that $G_1 = G_2 = 0$ is expected at $\omega = 0$. G_1 exhibits a single lobe (dash-dotted red lines), while G_2 grows monotonically to reach a maximum value at around $\omega \approx 2$, then decays in an oscillatory way (solid yellow lines). This is not the case in numerical results (blue crosses and purple circles), which are affected by the limited size of the numerical domain and present a finite $\bar{G}_{1,2}$ at $\omega = 0$. This can be quantified by deriving alternative semianalytical

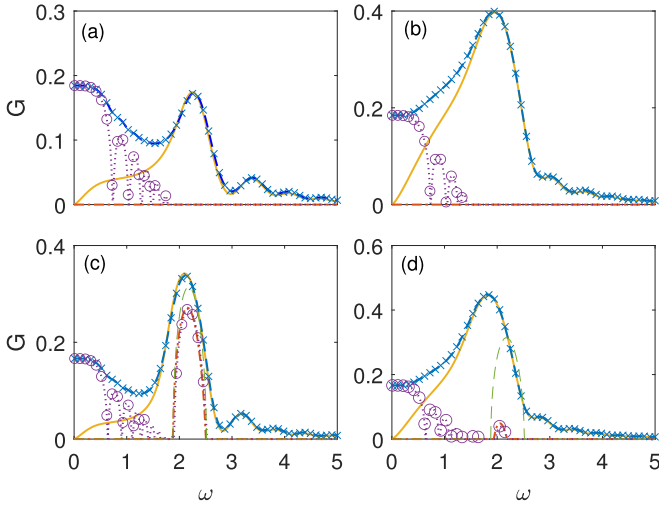


FIG. 3. MI gain curves for different values of \bar{L} and ε , for $\omega \geq 0$. (a) $\bar{L} = 1$, $\varepsilon = 0.2$; (b) $\bar{L} = 1$, $\varepsilon = 0.5$; (c) $\bar{L} = 1.15$, $\varepsilon = 0.2$; (d) $\bar{L} = 1.15$, $\varepsilon = 0.5$. Blue crosses (purple circles) represent \bar{G}_2 (\bar{G}_1) from numerical data, solid yellow (dash-dotted red) lines represent the theoretical estimates G_2 (G_1), dashed blue (dotted purple) lines represent the semianalytical estimates \tilde{G}_2 (\tilde{G}_1). In (c) and (d), we include the MI gain in the periodic case $\varepsilon = 0$ as a thin green dashed line.

estimates of gain. We notice that $T_-(L_N) \dots T_+(L_1) \approx \bar{T}^{N/2}$ [$M_-(L_N) \dots M_+(L_1) \approx \bar{M}^{N/2}$] and define

$$\tilde{G}_1 \equiv \frac{1}{N\bar{L}} \ln \left[\left(\bar{T}^{\frac{N}{2}} \right)_{11} + \left(\bar{T}^{\frac{N}{2}} \right)_{21} \right], \quad (14)$$

$$\tilde{G}_2 \equiv \frac{1}{2N\bar{L}} \ln \left[\left(\bar{M}^{\frac{N}{2}} \right)_{11} + \left(\bar{M}^{\frac{N}{2}} \right)_{21} \right], \quad (15)$$

where the matrix power is computed numerically and the subscripts refer to the corresponding numerically computed matrix elements. We notice in Fig. 3 that in every case, this estimate performs very well not only for $\omega \approx 0$, but in the whole domain.

In Figs. 3(a) and 3(b), $\bar{L} = 1 < 1.07$ and ε increases from 0.2 to 0.5. The MI is of purely stochastic origin. The local maximum value achieved by \bar{G}_2 at $\omega = \omega_{2,\max} > 0$, say $G_{2,\max}$, increases with ε and becomes of the same order of magnitude as the conventional MI (i.e., for constant anomalous GVD). The width of the sidelobes increases significantly as well.

In Figs. 3(c) and 3(d), $\bar{L} = 1.15 > 1.07$. There is thus a competition between the periodic and the stochastic effects. We also include the periodic-DM MI sidelobe for comparison (thin green dashed line).

For $\varepsilon = 0.2$ [Fig. 3(c)], the random fluctuations yield a broadened MI sidelobe. In contrast to the case of constant anomalous GVD perturbed by white noise, where the broadening is accompanied by a reduction of $G_{2,\max}$ [9], here this value is slightly enhanced. We also notice that \bar{G}_1 is always less than its periodic counterpart, consistently with Eq. (7). Comparison of Figs. 3(a) and 3(c) shows that the main sidelobe appearing in the former is located in the same region of the periodic sidelobe. The random fluctuations facilitate the

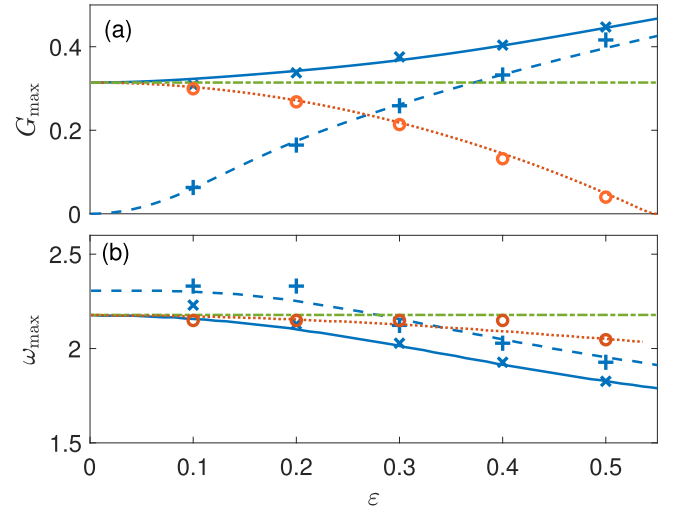


FIG. 4. (a) Maximum gain values and (b) their corresponding ω as a function of ε . The plus (cross) markers correspond to the maxima $G_{2,\max}$ for $\bar{L} = 1$ ($\bar{L} = 1.15$). The dashed (solid) blue lines correspond to the maxima of G_2 for $\bar{L} = 1$ ($\bar{L} = 1.15$). The green dash-dotted lines report, for reference, the constant values found in the periodic limit, i.e., the maxima of $G_1 = G_2$ for $\varepsilon = 0$. The red circles show the values of $G_{1,\max}$ and $\omega_{1,\max}$ for $\bar{L} = 1.15$, for which red dotted lines illustrate the corresponding maxima of G_1 . In (b), the line stops at $\varepsilon \approx 0.54$ (cutoff for G_1).

emergence of the MI sidelobes in a range that coincides with the periodic DM.

For a larger fluctuation ($\varepsilon = 0.5$), shown in Fig. 3(d), the residual effect of periodicity is completely erased and we obtain a single wide lobe similar to the corresponding below-threshold example of Fig. 3(b), but with a larger $G_{2,\max}$.

In order to summarize our findings, we show, in Figs. 4(a) and 4(b), respectively, $G_{j,\max}$ and the corresponding ω value, $\omega_{j,\max}$, with $j = 1, 2$, as a function of ε . Obviously, $G_{1,\max}$ is the local maximum value of \bar{G}_1 at $\omega = \omega_{1,\max} > 0$. We compare them to their corresponding theoretical estimates, i.e., the maxima of G_1 (G_2). Solid blue lines, crosses, red lines, and circles correspond to $\bar{L} = 1.15$, while dashed lines and pluses correspond to $\bar{L} = 1$. In Fig. 4(a), we notice that $G_{2,\max}$ increases monotonically with ε . As expected, for $\varepsilon \rightarrow 0$, the gain vanishes for $\bar{L} = 1$ and converges to the periodic $G_{1,\max} = 0.31$ (for $\varepsilon = 0$, dash-dotted green line) for $\bar{L} = 1.15$. For large ε , they converge to two very similar values, which is around 30% smaller than the conventional MI value. The dotted red line in Fig. 4(a) shows the maxima of G_1 obtained from Eq. (7). For $\varepsilon > 0.54$, $G_1 = 0$ for every ω . For this value of the fluctuation amplitudes, randomness completely overrules the effects of periodicity. This is corroborated by the values $G_{1,\max}$ (red circles), which match very well with the theoretical estimates (provided that a large enough N_{iter} is chosen). In Fig. 4(b), we observe that for both \bar{L} , $\omega_{2,\max}$ decreases with ε and converges to a value larger than the conventional MI value. Apart from numerical fluctuations, for $\bar{L} = 1.15$, $\omega_{2,\max} < \omega_{1,\max} < 2.18$, i.e., slightly below the $\varepsilon = 0$ value. For $\bar{L} = 1$, $\omega_{2,\max}$ is above its periodic counterpart and crosses it for $\varepsilon \approx 0.3$. The theoretical estimates work very well for every considered value of ε .

IV. CONCLUSIONS

To conclude, we investigated the effect of uniformly distributed random fluctuations of the *length* of the opposite GVD segments in DM fiber links. We considered the MI problem and developed an analytical technique to estimate the instability gain. The MI gain attains values comparable to the conventional ones in a homogeneous anomalous GVD fiber and up to 50% larger than those found for the periodic arrangement. Comparison to the direct numerical solution in a Monte Carlo fashion confirms the soundness of the method. Splicing tens of fiber segments of slightly different length and opposite GVD could allow one to experimentally demonstrate

this phenomenon. The number of samples obviously cannot be as large as that considered in our numerical analysis.

This may be of interest for tailoring and controlling MI sidebands for telecommunications and parametric sources.

ACKNOWLEDGMENTS

This research was supported by IRCICA (USR 3380 CNRS), Agence Nationale de la Recherche (Programme Investissements d’Avenir, I-SITE VERIFICO, Labex CEMPI); Ministry of Higher Education and Research; Hauts de France Council; and European Regional Development Fund (Photonics for Society P4S, Wavetech), CNRS (IPR LAFONI).

-
- [1] V. E. Zakharov and L. A. Ostrovsky, Modulation instability: The beginning, *Physica D* **238**, 540 (2009).
 - [2] T. B. Benjamin and J. E. Feir, The disintegration of wave trains on deep water, Part I. Theory, *J. Fluid Mech.* **27**, 417 (1967).
 - [3] V. E. Zakharov, Stability of periodic waves of finite amplitude on the surface of a deep fluid, *J. Appl. Mech. Tech. Phys.* **9**, 190 (1968).
 - [4] V. I. Bespalov and V. I. Talanov, Filamentary structure of light beams in nonlinear liquids, *Zh. Pis ma Redaktsiiu* **3**, 471 (1966).
 - [5] K. Tai, A. Hasegawa, and A. Tomita, Observation of Modulational Instability in Optical Fibers, *Phys. Rev. Lett.* **56**, 135 (1986).
 - [6] S. B. Cavalcanti, J. C. J. C. Cressoni, H. R. da Cruz, and A. S. Gouveia-Neto, Modulation instability in the region of minimum group-velocity dispersion of single-mode optical fibers via an extended nonlinear Schrödinger equation, *Phys. Rev. A* **43**, 6162 (1991).
 - [7] F. Biancalana and D. V. Skryabin, Vector modulational instabilities in ultra-small core optical fibres, *J. Opt. A: Pure Appl. Opt.* **6**, 301 (2004).
 - [8] N. J. Smith and N. Doran, Modulational instabilities in fibers with periodic dispersion management, *Opt. Lett.* **21**, 570 (1996).
 - [9] F. K. Abdullaev, S. A. Darmanyan, A. Kobayakov, and F. Lederer, Modulational instability in optical fibers with variable dispersion, *Phys. Lett. A* **220**, 213 (1996).
 - [10] M. Droques, A. Kudlinski, G. Bouwmans, G. Martinelli, and A. Mussot, Experimental demonstration of modulation instability in an optical fiber with a periodic dispersion landscape, *Opt. Lett.* **37**, 4832 (2012).
 - [11] A. Armaroli and F. Biancalana, Tunable modulational instability sidebands via parametric resonance in periodically tapered optical fibers, *Opt. Express* **20**, 25096 (2012).
 - [12] A. Mussot, M. Conforti, S. Trillo, F. Copie, and A. Kudlinski, Modulation instability in dispersion oscillating fibers, *Adv. Opt. Photon.* **10**, 1 (2018).
 - [13] F. K. Abdullaev and J. Garnier, Modulational instability of electromagnetic waves in birefringent fibers with periodic and random dispersion, *Phys. Rev. E* **60**, 1042 (1999).
 - [14] J. Garnier and F. K. Abdullaev, Modulational instability induced by randomly varying coefficients for the nonlinear Schrödinger equation, *Physica D* **145**, 65 (2000).
 - [15] M. Chertkov, I. Gabitov, and J. Moeser, Pulse confinement in optical fibers with random dispersion, *Proc. Natl. Acad. Sci. USA* **98**, 14208 (2001).
 - [16] G. Dujardin, A. Armaroli, S. R. Nodari, A. Mussot, A. Kudlinski, S. Trillo, M. Conforti, and S. De Bievre, Modulational instability in optical fibers with randomly kicked normal dispersion, *Phys. Rev. A* **103**, 053521 (2021).
 - [17] A. Armaroli, G. Dujardin, A. Kudlinski, A. Mussot, S. Trillo, S. De Bièvre, and M. Conforti, Stochastic modulational instability in the nonlinear Schrödinger equation with colored random dispersion, *Phys. Rev. A* **105**, 013511 (2022).
 - [18] G. P. Agrawal, *Nonlinear Fiber Optics*, 5th ed. (Academic Press, Oxford, 2012), p. 648.
 - [19] S. K. Turitsyn, B. G. Bale, and M. P. Fedoruk, Dispersion-managed solitons in fibre systems and lasers, *Phys. Rep.* **521**, 135 (2012).
 - [20] J. C. Bronski and J. Nathan Kutz, Modulational stability of plane waves in nonreturn-to-zero communications systems with dispersion management, *Opt. Lett.* **21**, 937 (1996).
 - [21] B. A. Malomed and A. Berntson, Propagation of an optical pulse in a fiber link with random-dispersion management, *J. Opt. Soc. Am. B* **18**, 1243 (2001).
 - [22] N. Van Kampen, *Stochastic Processes in Physics and Chemistry* (Elsevier, Amsterdam, 2007).
 - [23] <https://www.wolfram.com/mathematica/>.
 - [24] M. Farahmand and M. de Sterke, Parametric amplification in presence of dispersion fluctuations, *Opt. Express* **12**, 136 (2004).